Transport properties of the two-dimensional electron gas in $Al_xGa_{1-x}N$/GaN heterostructures

2007 J. Phys.: Condens. Matter 19 046204

(http://iopscience.iop.org/0953-8984/19/4/046204)

INSTITUTE OF PHYSICS PUBLISHING JOURNAL OF PHYSICS: CONDENSED MATTER

J. Phys.: Condens. Matter **19** (2007) 046204 (11pp) doi:10.1088/0953-8984/19/4/046204

Transport properties of the two-dimensional electron gas in $Al_xGa_{1-x}N$/GaN heterostructures

Xiuxun Han[1,2], Yoshio Honda[1], Tetsuo Narita[1], Masahito Yamaguchi[1] and Nobuhiko Sawaki[1]

[1] Department of Electronics and Akasaki Research Center, Nagoya University, Chikusa-ku, Nagoya, 464-8603, Japan
[2] Venture Business Laboratory, Nagoya University, Chikusa-ku, Nagoya, 464-8603, Japan

E-mail: xxhan@vbl.nagoya-u.ac.jp

Received 8 September 2006, in final form 29 December 2006
Published 12 January 2007
Online at stacks.iop.org/JPhysCM/19/046204

Abstract

Magnetotransport measurements were performed on a series of $Al_xGa_{1-x}N$/GaN heterostructures with different Al compositions ($x = 0.15$, 0.20 and 0.30) at 4.2 K. Adopting a fast Fourier transform method, we analysed the Shubnikov–de Hass oscillations due to the two-dimensional electron gas to derive the quantum scattering time (τ_q). It was found that the quantum scattering time in the ground subband decreases with increasing Al composition: 0.194 ps ($x = 0.15$), 0.174 ps ($x = 0.20$) and 0.123 ps ($x = 0.30$), respectively. To discern the predominant scattering process, the scattering time limited by interface roughness, the residual impurity and the alloy disorder were investigated numerically by including inter-subband scattering. We found that enhanced interface roughness scattering dominates both the transport and quantum scattering time in the ground subband.

1. Introduction

$Al_xGa_{1-x}N$/GaN heterostructures have attracted much attention because of their potential use in high-power and high-frequency electronic devices [1]. Even in the absence of intentional doping, a two-dimensional electron gas (2DEG) with a typical density of $\sim 10^{13}$ cm^{-2} can be formed at the $Al_xGa_{1-x}N$/GaN hetero-interface due to the high field induced by spontaneous and/or piezoelectric polarization. It has been shown that a high Al composition in the $Al_xGa_{1-x}N$ barrier layer leads to a significant increase in the electron density [2–4], which may benefit the realization of high-power-density electronic devices. However, the mobility has been found to decrease with an increase in the Al composition [2].

Various scattering processes are responsible for the low mobility of the 2DEG in $Al_xGa_{1-x}N$/GaN heterostructures, such as interface roughness, alloy disorder and defects originating from the large lattice mismatch between the top $Al_xGa_{1-x}N$ layer and the GaN

underlayer [5]. Only recently, the population of the second subband in an $Al_{0.22}Ga_{0.78}N$/GaN heterostructure was observed by magnetoresistance measurement [6]. The occupation of multi-subbands will open a new scattering channel (intersubband scattering), as discussed by Tang *et al* [7]. Those novel features require detailed investigations of the relationship between the structural factors and the transport parameters of $Al_xGa_{1-x}N$/GaN 2DEGs with different Al compositions. In the analysis of the scattering phenomena, the leading parameter will be the transport scattering time (τ_t) which should be deduced by Hall measurements. In addition to the transport scattering time, analysis of the quantum scattering time (τ_q) is proved to be a powerful tool for discerning the dominant scattering mechanisms underlying the transport behaviours [8, 9]. The quantum scattering time τ_q can be extracted from the magnitude of the Shubnikov–de Hass (SdH) oscillation and characterizes the time that a carrier remains in a particular momentum eigenstate in the presence of a perturbing potential [10]. In general, if large angle scattering events are dominant, the magnitude of the transport scattering time should be equal to the quantum scattering time, that is, the ratio between τ_t and τ_q is close to unity. However, a large difference between them occurs if small angle scattering events are dominant.

For the $Al_xGa_{1-x}As$/GaAs system, modulation doping plays the key role in realizing a high-density 2DEG. Remote donor scattering is recognized as the dominant long-range scattering mechanism at low temperatures [10, 11]. In an $Al_xGa_{1-x}N$/GaN heterostructure, however, surface donor states are suggested to provide electrons [12] and the density of background donors is believed to be much lower ($\sim 10^{16}$ cm^{-3}) than that of intentional doping. Limited work has been published and the major source of the scattering events in an $Al_xGa_{1-x}N$/GaN heterostructure is still under discussion.

Manfra *et al* [13] investigated the density dependences of two scattering times and suggested that charged dislocation, rather than remote donors, determines both scattering times. It should be noted that their samples have a relatively low electron density (ranging from 2×10^{11} to 2×10^{12} cm^{-2}). Using roughness parameters determined by atomic force microscopy (AFM) images, Tang *et al* [14] studied the scattering time in samples grown by molecular beam epitaxy (MBE) and concluded that the quantum scattering time is dominated by interface roughness scattering while the transport scattering time is dominated by other short-range scattering mechanisms. Cho and his co-workers [15] showed that interface roughness scattering plays the key role in both scattering times in samples made by metalorganic vapour phase epitaxy (MOVPE). In those two reports, both the magnitude of the roughness amplitude (Δ) and the lateral correlation length (Λ) were different from each other: in MBE samples Δ was larger than 10 nm and Λ of the order of several hundreds of nanometres, while in the MOVPE samples, Δ and Λ were as short as $\sim$4 Å and $\sim$12 nm, respectively. Though different growth methods and/or surface treatments might be the reason, accurate determination of the interface roughness parameters is still difficult.

In a previous paper, magnetotransport was investigated on a series of $Al_xGa_{1-x}N$/GaN samples grown by MOVPE [16]. We found that the quantum scattering time depends on the Al composition. In this paper, changes in the subband structure and the quantum scattering time are analysed in detail by adopting numerical fitting procedures. The dominant scattering mechanisms are characterized as a function of the Al composition. We show that interface roughness scattering plays a key role in both the transport and quantum scattering times.

2. Experimental process and results

An $Al_xGa_{1-x}N$/GaN heterostructure was grown on a c-plane sapphire substrate by the low-pressure MOVPE method. It consisted of a nominally undoped 1 μm GaN layer and a

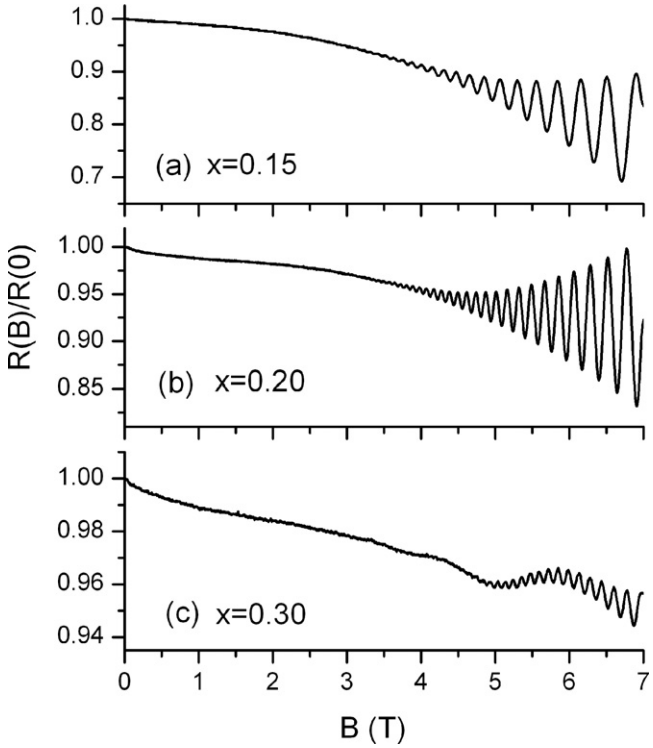

Figure 1. SdH oscillations of three undoped $Al_xGa_{1-x}N$/GaN heterostructures. The magnetoresistances are normalized. The oscillation has a single periodicity in both samples with $x = 0.15$ and 0.20, while a double periodical one is observed in the sample with $x = 0.30$.

nominally undoped 20 nm thick $Al_xGa_{1-x}N$ layer grown at 1080 °C. More details of the growth condition have been described previously [16]. For convenience, three samples with Al compositions of 0.15, 0.20 and 0.30 are numbered as samples 1, 2 and 3, respectively. Evaporated Ti/Al/Ti/Au (20/100/45/55 nm) was treated in N_2 ambient at 800 °C for 30 s to form an ohmic contact on the sample surface. Low-field Hall measurements were performed to obtain the temperature dependent mobilities (from 16 to 300 K). The mobility decreased from 6640 to 3810 $cm^2\ V^{-1}\ s^{-1}$ at 16 K as the Al composition increased from 0.15 to 0.30 [16].

The van der Pauw configuration and the standard ac lock-in technique were used in the SdH oscillation measurement at 4.2 K. We kept the ac bias current less than 0.5 μA to avoid sample heating. Magnetic fields up to 7 T were applied perpendicular to the sample surface. Obvious SdH oscillations were observed in the longitudinal magnetoresistance of all three samples [16]. Measurement results are reproduced in figure 1. The onset of oscillation at a field as low as about 3.5 T indicates the good quality of our 2DEG structure. Oscillations of sample 1 and sample 2 are much stronger than that of sample 3, which is in accordance with the magnitude of the low-temperature mobilities. A noticeable feature of sample 3 is the double periodical oscillation, which indicates an additional contribution from the higher subband in this sample.

Replotting the magnetoresistance as a function of the reciprocal magnetic field $(1/B)$ and performing a fast Fourier transform (FFT), one can calculate the electron concentration n_i at

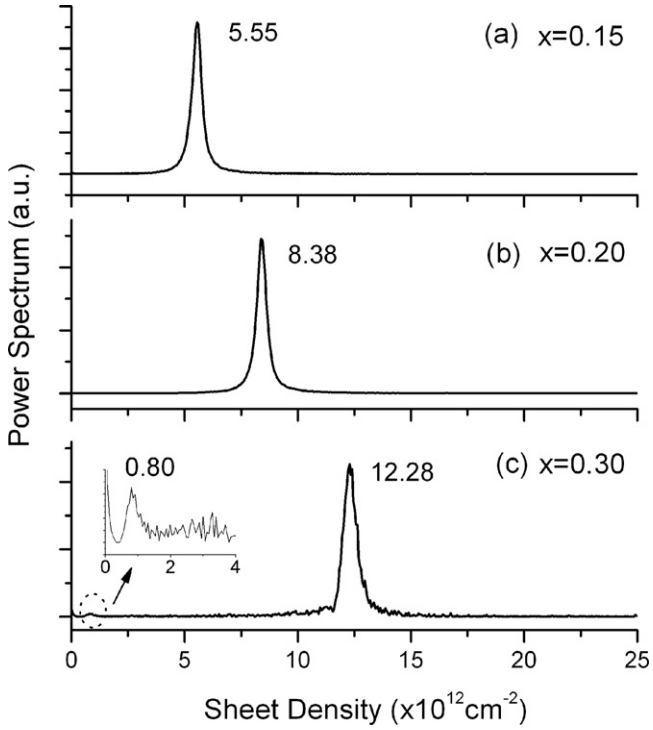

Figure 2. Fast Fourier transform spectra of SdH oscillations observed in figure 1. The frequency has been converted to the corresponding sheet electron density.

the ith subband by [17]

$$n_i = (2e/h)[1/\Delta(1/B)] = m^*(E_f - E_i)/\pi\hbar^2, \tag{1}$$

where $\Delta(1/B)$ is the period of the SdH oscillations and $E_f - E_i$ is the energy difference between the Fermi level and the energy level of the ith subband. The FFT power spectra of SdH oscillations for three samples are shown in figure 2, where the frequency has been converted to the sheet electron density n_i according to equation (1). It can be seen that for samples 1 and 2 only one peak is found with sheet densities recorded as 5.55 and 8.38×10^{12} cm^{-2}, respectively. Apparently, only one subband is occupied by electrons in samples 1 and 2. In sample 3, we found a small peak at the low density of 0.80×10^{12} cm^{-2} in addition to the main peak at 12.28×10^{12} cm^{-2}. This shows that the second subband is occupied in this particular sample. Assuming an effective mass of 0.22 m_0, the energy difference between the first two subbands is deduced to be 125 meV.

The quantum scattering time can be determined from the Dingle plot [11]. Accordingly, the amplitude ΔR of the SdH oscillations is given by

$$\Delta R = 4R_0X(T)\exp(-\pi/\omega_c\tau_q), \tag{2}$$

where R_0 is the zero-field resistance, τ_q the quantum scattering time, $\omega_c(=eB/m^*)$ is the cyclotron frequency and $X(T)$ follows

$$X(T) = (2\pi^2 k_B T/\hbar\omega_c)/\sinh(2\pi^2 k_B T/\hbar\omega_c). \tag{3}$$

Thus, by plotting $\ln(\Delta R/R_0X(T))$ against $1/B$, the slope gives $1/\tau_q$ and leads directly to the quantum scattering time.

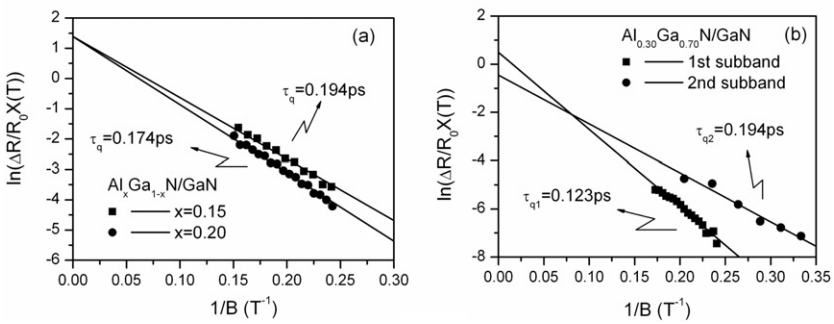

Figure 3. (a) Dingle plots for samples with an Al composition of 0.15 and 0.20. Both lines pass the theoretical intercept ln 4. (b) Dingle plots of two subbands for the sample with an Al composition of 0.30. Lower intercepts are observed due to intersubband scattering effects.

Table 1. Electron densities and transport parameters derived from experimental data.

Al composition (x)	n (10^{12} cm^{-2}, 4.2 K)	μ (cm^2 V^{-1} s^{-1}, 16 K)	τ_q (ps, 4.2 K)
0.15	5.55	6640	0.194
0.20	8.38	5690	0.174
0.30	12.28 (1st subband)	3810	0.123 (1st subband)
	0.80 (2nd subband)		0.194 (2nd subband)

In order to analyse the oscillatory part ΔR, FFT band-pass techniques were used to remove the background and also to separate contributions from different subbands [16]. Dingle plots of samples 1 and 2 are given in figure 3(a). Both sets of data trace the linear behaviours with intercept of ln 4. Following the relationship described in equation (2) we get a quantum scattering time of 0.194 ps for sample 1 and 0.174 ps for sample 2 from corresponding slopes. Dingle plots for sample 3 are shown in figure 3(b). One can note that both intercepts are less than ln 4, but the intercept for the ground subband is higher than that of the second subband. This is in agreement with Coleridge's theoretical suggestion [18] that, on the limit of $n_2 \ll n_1$, the intercept for the second subband is essentially determined by the amount of intersubband scattering and it will be less than ln 2. For the ground subband, the intercept should also be near but less than ln 4. From the slopes, we obtain that τ_q of the second subband is 0.194 ps, a little longer than that of the ground subband, 0.123 ps.

Electron densities and transport parameters derived from experimental data are summarized in table 1. Obviously, with the increase in Al composition the electron density shows a rapid increase, while the quantum scattering time of the ground subband decreases remarkably. The ratio of τ_t to τ_q in the present samples is estimated to be ∼4, which is much lower than the 16–24 reported by Manfra *et al* [13], where the charged dislocation scattering is believed to play the key role as the electron density is less than 2×10^{12} cm^{-2}. The small ratio in our sample suggests that long-range impurity scattering might not be predominant. If alloy scattering dominates the transport, on the other hand, its short-range nature should restrict τ_t/τ_q to unity, which is not the case in our samples under study. There might also be important scattering from the interface roughness. In order to evaluate its contribution, the roughness parameters of $Al_xGa_{1-x}N$/GaN are required, and these are not easy to determine experimentally. In this study, we attempt to evaluate them by investigating the temperature dependent mobility numerically. The roughness amplitude and lateral correlation length are treated as adjustable parameters to fit the experimental data.

3. Numerical evaluation of the scattering processes

According to the scattering theory related to 2DEGs of III–V semiconductors [19, 20], the scattering rate can be given by

$$\frac{1}{\tau} = \int_0^{\pi} Q(\theta) f(\theta)\, \mathrm{d}\theta \tag{4}$$

where $Q(\theta)$ is proportional to the scatting probability due to individual scattering events through the scattering angle θ; $f(\theta) = 1$ for quantum scattering time and $f(\theta) = 1 - \cos(\theta)$ for transport scattering time, respectively. In our calculation we considered all important scattering events, which include elastic scattering due to alloy disorder, interface roughness, ionized impurities, piezoelectric and deformational potential acoustic phonons and inelastic scattering due to polar optical phonons.

For the elastic case, we calculated the scattering time numerically by using the accurate wavefunctions, which are obtained by solving the Schrödinger and Poisson equations self-consistently [21]. In this framework, we can easily include the inter-subband scattering due to the occupation of the upper subbands. In the present calculations, we considered the ground and the second subband. For polar optical phonon scattering, accurate calculation requires direct solution of the linearized Boltzmann equation using an iteration method [22]. However, Gelmont *et al* [23] developed an approximate momentum relaxation rate for 2DEGs which can be used to estimate the polar optical mobility for a wide temperature range. Here we use this analytical form for simplicity. Because the polar optical phonon scattering mainly suppresses high-temperature mobilities, this approximation will be acceptable for our interest in the present study. A detailed formulation related to each scattering event is available from [20, 24–27].

The total scattering time can be obtained by combining individual events following Matthiessen's rule

$$1/\tau_i = \sum_n 1/\tau_n, \tag{5}$$

and the Hall mobility μ is defined by

$$\mu = \frac{\sum_i n_i \mu_i^2}{\sum_i n_i \mu_i}, \tag{6}$$

where the transport mobility of electrons in the ith subband is defined as $\mu_i = e\tau_i/m^*$.

In the case of $Al_xGa_{1-x}As$/GaAs heterostructures, heavy doping in the barrier layer is critical to realizing a high density of 2DEGs. Thus the remote ionized donors are traditionally treated as the dominant scattering mechanism. In contrast, the spontaneous and piezoelectric polarization fields act as the driving force to form 2DEGs in $Al_xGa_{1-x}N$/GaN heterostructures. In our calculation, we only considered the scattering from residual impurities. For alloy scattering, we used a scattering potential of 1.8 eV, which was derived through measurement by Jena *et al* [28]. Finally, we left interface roughness amplitude and lateral correlation length as two adjustable parameters to provide a good fit to the experimental data. Other material parameters used during the calculation are listed in table 2.

When solving the Schrödinger and Poisson equations, we assumed that 2DEGs were from the donor-like surface states. The calculated 2DEG concentrations were about 5.49, 8.18 and 13.74×10^{12} cm^{-2} for samples 1, 2 and 3, respectively, which were comparable to the SdH measurement results.

Figure 4 shows the total numerical mobility for sample 1 as a function of the lateral correlation length Λ for three different roughness amplitudes $\Delta = 1$, 3 and 5 Å at 4.2 K. For a given Δ, the calculated mobility first shows a rapid decrease with increasing Λ and then

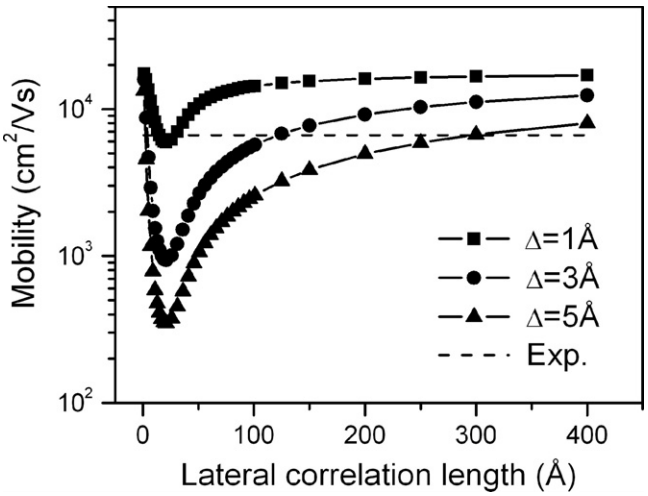

Figure 4. Calculated total mobility of $x = 0.15$ as a function of lateral correlation length Λ for three different roughness amplitudes $\Delta = 1, 3, 5$ Å at 4.2 K. The dashed line is the experimental mobility of sample 1 at 16 K.

Table 2. Material constants used during calculation.

GaN	
Effective mass, m^* (m_0)	0.22 [34]
Static dielectric constants, ε_s (ε_0)	8.9 [33]
High-frequency dielectric constant, ε_∞ (ε_0)	5.35 [33]
Density (10^3 kg m^{-3})	6.1 [36]
Elastic constants CL (10^{11} N m^{-2})	2.66 [36]
CT (10^{11} N m^{-2})	0.62 [36]
Deformation potential (eV)	8.5 [36]
LO phonon energy (meV)	91.8 [33]
Piezoelectric constant (10^9 V m^{-1})	4.28 [36]
$Al_xGa_{1-x}N$	
Static dielectric constants (ε_0)	$-0.4x + 8.9$ [33]
Effective mass, m^* (m_0)	$0.33x + 0.22(1 - x)$ [34]
Band offset (eV)	$0.7(2.12x + 0.6x^2)$ [35]

increases moderately to a saturation value at which alloy scattering becomes dominant. The dashed line is the measured Hall mobility of the sample 1 at 16 K. As can be seen, more than one set of Δ and Λ can fit the experimental data well. But, if Δ is much less than $\sim$1 Å, large deviations to the measured mobility will occur at any Λ. For large Δ, on the other hand, a value of several hundreds of angstroms for Λ is required to get good agreement with the measured mobility. This, however, is much longer than the effective scattering length given by $\Lambda \approx \pi/2k_F$ [29], where k_F is the Fermi wavevector. Actually, assuming $k_F = (2\pi n)^{1/2}$, the effective scattering length is estimated to be $\Lambda = 20$–30 Å in sample 1. This range is comparable with the values adopted by other workers in their simulations [22, 30]. Since no reliable Λ can be referred from experiments, in the following calculation we will consider this effective scattering case and set the lateral correlation length to 30 Å. The roughness amplitude Δ is treated as the adjustable parameter to fit the temperature dependent mobilities. If values

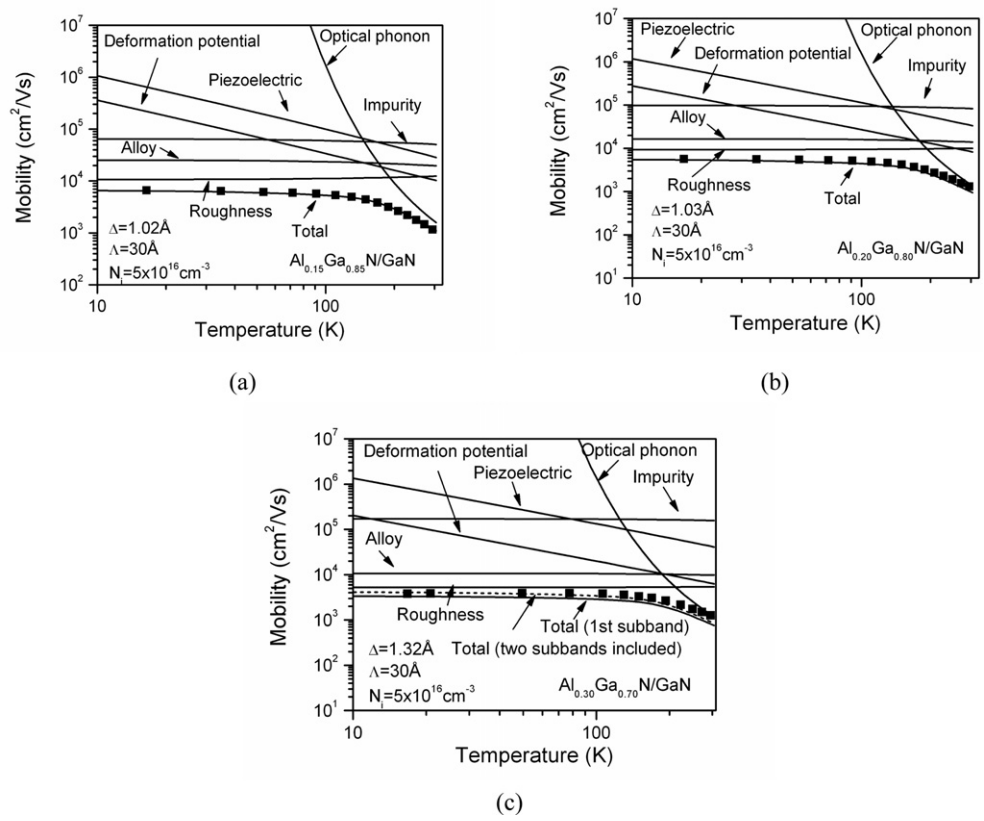

Figure 5. Calculated mobilities of 2DEGs as a function of temperature (4.2–305 K) with (a) $x = 0.15$, (b) $x = 0.20$ and (c) $x = 0.30$. Experimental data are also shown as solid squares. N_i is the concentration of ionized residual impurities. In (c), the dashed line is the total mobility calculated by taking both occupied subbands into account, and the solid lines are related to the ground subband.

other than 30 Å are used for Λ, one can expect from figure 4 that good fitting values for Δ will be modified accordingly. But this small shift will not impede the predominant scattering mechanism.

In figure 5(a) we plot the calculated mobilities and the experimental results for sample 1. In this case an excellent agreement is obtained with $\Delta = 1.02$ Å over the whole temperature range. Alloy scattering is not so significant in this sample. Interface roughness scattering obviously dominates at low temperatures. At high temperatures, strong scattering from phonons leads to rapid decrease in the mobility. A similar tendency can be seen for samples 2 and 3 (figures 5(b), (c)). For sample 3, the contribution of the second subband has been included in the calculation (dashed line in figure 5(c)). Other solid lines are related to the ground subband. With the increase of Al composition and electron density, alloy scattering shows an increased contribution but still less than that of interface roughness scattering. Good agreements with the experimental data can be found with $\Delta = 1.03$ and 1.32 Å for samples 2 and 3, respectively. During the calculation, we set the residual impurity concentration N_i to 5×10^{16} cm^{-3}. This value is comparable to the reported concentration of residual impurities in undoped high-quality GaN [31, 32]. Numerical results shown in figure 5 show that the contribution from ionized residual impurities at low temperature is negligible if we use the value $N_i = 5 \times 10^{16}$ cm^{-3}.

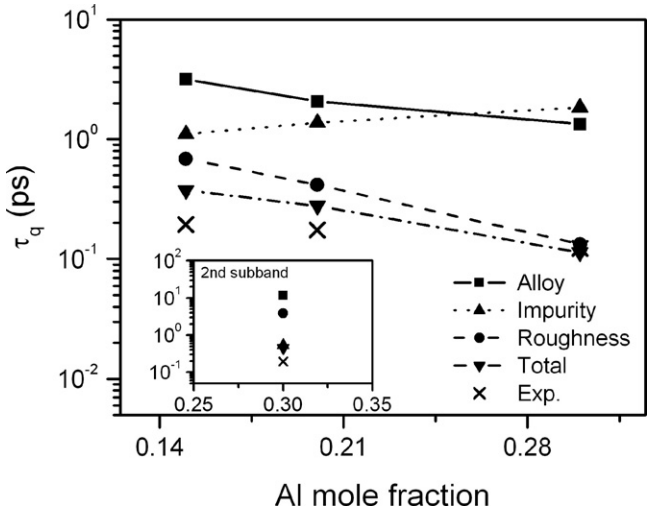

Figure 6. Calculated quantum scattering time of electrons in the ground subband at 4.2 K for three samples with $x = 0.15$, 0.20 and 0.30. Measurement results are denoted as crosses for comparison. The inset shows the calculated results of the second subband as $x = 0.30$. During the calculation, N_i is assumed to be 5×10^{16} cm^{-3}.

However, residual impurity concentration usually strongly depends on the experiment and/or growth conditions. If the residual impurity concentration is increased to 10^{17} cm^{-3}, the corresponding mobility will decrease to 32 428, 49 044, and 85 645 cm^2 V^{-1} s^{-1} for samples 1, 2 and 3, respectively. These values will not reduce the total mobility significantly because they are still much larger than the experimental values. Further increase of the residual impurity concentration to ($N_i > 5 \times 10^{17}$ cm^{-3}) will result in a low mobility in the sample with low electron density, where the screening effect is weak. The proper range of the residual impurity concentration for our samples will be discussed shortly.

By using the roughness parameters obtained from fitting results, we calculated the quantum scattering time at 4.2 K. Results are depicted in figure 6 together with the experimental data (denoted as crosses). Although a small deviation occurs at low Al compositions, theoretical values are comparable to the experimental data. It is shown that interface roughness scattering predominates over the other two scattering mechanisms and determines τ_q at low temperatures. The behaviour of the roughness amplitude parameters deduced from fitting results reveals that Δ has a similar value for samples with $x = 0.15$ and 0.20. Thus, the interface morphology does not seem to change much as the Al composition increases in that range. For $x = 0.30$, however, Δ increases to 1.32 Å, which indicates degradation of the interface morphology. That may be due to the rise in tensile strain in the barrier with high Al composition. Similar phenomena are also observed experimentally [3]. To know the details of the roughness parameters as a function of the Al composition, however, further analyses of the interface morphology by transmission electron microscopy (TEM) or AFM are desirable.

We note that τ_q for the second subband is smaller than that for the first subband in sample 3. In contrast to the ground subband, the electron density in the second subband is very low. Moreover, the wavefunction of the second subband is less localized to the interface. A large part extends into the GaN layer. One can expect that scattering from interface roughness is much weaker in the second subband than that of the ground subband. In the inset of figure 6 we give the calculated quantum scattering time of electrons in the second subband at 4.2 K.

It can be seen that residual impurity scattering overwhelms interface roughness scattering and dominates τ_q of electrons dwelling in the second subband.

The above discussions about τ_q have been based on the assumption that the residual impurity density is $N_i = 5 \times 10^{16}$ cm^{-3}. If we increase N_i to 10^{17} cm^{-3}, the parameters adopted for the interface roughness should still be valid. But the scattering time limited by the residual impurity will be reduced to about a half of the value shown in figure 6. Nevertheless, good fitting is available to the experimental τ_q for three samples. We might conclude that, for sample 1, the quantum scattering time is determined by the interface roughness and residual impurity scattering jointly. In samples with higher Al composition, the interface roughness scattering still dominates. If other values much higher than 10^{17} cm^{-3} are adopted for N_i, obvious deviations occur between calculated and experimental values of τ_q, especially for the second subband of sample 3. Thus, the proper range of residual impurity concentration is expected to lie in the region of about 5×10^{16}–1×10^{17} cm^{-3} for our samples.

4. Summary

We have investigated the electron transport in nominally undoped $Al_xGa_{1-x}N$/GaN heterostructures with different Al compositions at 4.2 K. With increase in the Al composition, the quantum scattering time of the ground subband is determined to be 0.194–0.123 ps, depending on the Al composition. By fitting the calculated temperature dependent mobility to the experimental data, we obtained the roughness amplitude and the lateral correlation length that could lead to the good agreement. We find that the enhanced interface roughness scattering with increase in the Al composition plays the key role in the transport behaviours of the ground subband of the 2DEG in our samples.

Acknowledgment

This work was partly supported by a Grant-in-Aid from the Japan Society for the Promotion of Science.

References

[1] Pearton S J, Ren F, Zhang A P and Lee K P 2000 *Mater. Sci. Eng.* R **30** 55
[2] Keller S, Parish G, Fini P T, Heikman S, Chen C-H, Zhang N, DenBaars S P, Mishra U K and Wu Y-F 1999 *J. Appl. Phys.* **86** 5850
[3] Miyoshi M, Egawa T and Ishikawa H 2005 *J. Vac. Sci. Technol.* B **23** 1527
[4] Jogai B 2003 *J. Appl. Phys.* **93** 1631
[5] Hsu L and Walukiewicz W 2001 *J. Appl. Phys.* **89** 1783
[6] Zheng Z W, Shen B, Zhang R, Gui Y S, Jiang C P, Ma Z X, Zheng G Z, Guo S L, Shi Y, Han P, Zheng Y D, Someya T and Arakawa Y 2000 *Phys. Rev.* B **62** R7739
[7] Tang N, Shen B, Zheng Z W, Liu J, Chen D J, Lu J, Zhang R, Shi Y, Zheng Y D, Gui Y S, Jiang C P, Qiu Z J, Guo S L, Chu J H, Hoshino K, Someya T and Arakawa Y 2003 *J. Appl. Phys.* **94** 5420
[8] Das B, Subramaniam S, Melloch M R and Miller D C 1993 *Phys. Rev.* B **47** 9650
[9] Wang T, Bai J, Sakai S, Ohno Y and Ohno H 2000 *Appl. Phys. Lett.* **76** 2737
[10] Das Sarma S and Stern F 1985 *Phys. Rev.* B **32** 8442
[11] Coleridge P T 1991 *Phys. Rev.* B **44** 3793
[12] Ibbetson J P, Fini P T, Ness K D, DenBaars S P, Speck J S and Mishra U K 2000 *Appl. Phys. Lett.* **77** 250
[13] Manfra M J, Simon S H, Baldwin K W, Sergent A M, West K W, Molnar R J and Caissie J 2004 *Appl. Phys. Lett.* **85** 5278
[14] Tang H, Webb J B, Coleridge P, Bardwell J A, Ko C H, Su Y K and Chang S J 2002 *Phys. Rev.* B **66** 245305
[15] Cho H-I, Gusev G M, Kvon Z D, Renard V T, Lee J-H and Portal J-C 2005 *Phys. Rev.* B **71** 245323

[16] Han X, Honda Y, Narita T, Yamaguchi M and Sawaki N 2006 *IWN2006: Extended Abstract of International Workshop on Nitride Semiconductors (Tyoko)*; *Phys. Status Solidi* at press
[17] Chang C-S, Fetterman H R and Viswanathan C R 1989 *J. Appl. Phys.* **66** 928
[18] Coleridge P T 1990 *Semicond. Sci. Technol.* **5** 961
[19] Gold A 1988 *Phys. Rev.* B **38** 10798
[20] Walukiewicz W, Ruda H E, Lagowski J and Gatos H C 1984 *Phys. Rev.* B **30** 4571
[21] Han X, Li J, Wu J, Cong G, Liu X, Zhu Q and Wang Z 2005 *Physica* E **28** 230
[22] Yu T-H and Brennan K F 2001 *J. Appl. Phys.* **89** 3827
[23] Gelmont B L, Shur M and Stroscio M 1995 *J. Appl. Phys.* **77** 657
[24] Hirakawa K and Sakaki H 1986 *Phys. Rev.* B **33** 8291
[25] Ando T 1982 *J. Phys. Soc. Japan* **51** 3900
[26] Mori S and Ando T 1979 *Phys. Rev.* B **19** 6433
[27] Price P J 1982 *Surf. Sci.* **113** 199
[28] Jena D, Heikman S, Speck J S, Gossard A, Mishra U K, Link A and Ambacher O 2003 *Phys. Rev.* B **67** 153306
[29] Sakaki H, Noda T, Hirakawa K, Tanaka M and Matsusue T 1987 *Appl. Phys. Lett.* **51** 1934
[30] Zanato D, Gokden S, Balkan N, Ridley B K and Schaff W J 2004 *Semicond. Sci. Technol.* **19** 427
[31] Nakamura S 1991 *Japan. J. Appl. Phys.* **30** L1705
[32] Wu Y-F, Keller B P, Keller S, Kapolnek D, Kozodoy P, Denbaars S P and Mishra U K 1996 *Appl. Phys. Lett.* **69** 1438
[33] Harima H 2002 *J. Phys.: Condens. Matter* **14** R967
[34] Majewski J A, Stadele M and Vogl P 1997 *Mater. Res. Soc. Symp. Proc.* **449** 887
[35] Vurgaftman I, Meyer J R and Ram-Mohan L R 2001 *J. Appl. Phys.* **89** 5815
[36] Hsu L and Walukiewicz W 1997 *Phys. Rev.* B **56** 1520